A NEW CFD-BASED APPROACH TO DESIGNING WATER PURIFICATION DEVICES

Edoardo Sech[1], Anna Stoppato[1], Alberto Benato[1*]

[1] Dipartimento di Ingegneria Industriale, Università degli Studi di Padova, Padova, Italy

*Corresponding Author: alberto.benato@unipd.it

ABSTRACT

Access to safe water, sanitation, and hygiene is the most basic human need for health and well-being. People will lack access to this basic service in the future, unless advances in water purification are achieved. Precisely from this perspective, hydrodynamic cavitation has been recognised by researchers as a potentially first-rate technology in this field. Hydrodynamic cavitation (HC) is an advanced oxidation technique that has found numerous applications in recent years, from wastewater treatment to the synthesis of nanoparticles. Cavitation identifies the appearance of vapour cavities inside an initially homogeneous liquid medium. Bubble formation and growth are due to a sharp decrease in local pressure below saturation conditions. Subsequent bubble collapse releases a large amount of energy. Extreme conditions promote the breakdown of substances. The aim of this work is to explore the possibility of integrating this technology in industrial processes. The partial or total substitution of traditional, expensive, and energy-consuming water purification methods by HC is driven by its competitive cost-effectiveness and high energy efficiency. Referring to the configurations for cavitation promotion, Venturi shaped nozzles have been chosen, as generating more cavities for the same pressure drops, thanks to their smooth section change. In addition to that, Venturi tubes can couple more freedom in design, because of the larger number of geometrical parameters involved, to an elementary shape. The spread of this kind of technology at the industrial level found a major obstacle in the lack of a consistent design and optimisation procedure. With the aim of solving the literature lack mentioned above, the master tool for optimisation is Computational Fluid Dynamics (CFD) analysis, allowing one to investigate the phenomenon and clarify the effects of the geometry changes. To do so, a fluid model was elaborated that is suitable for a precise definition of the main performance of a cavitating configuration, which still limits computational effort. However, a critical look is taken to the definition of a satisfactory meshing phase to properly appreciate the deep cavitating wall-bounded flow. A subsequent calibration of the model is implemented using experimental data taken from the literature. Once the consistency of the model was established, it was possible to study a new configuration aimed at simplifying the manufacturing process and implementing a possible multireactor device. Despite a minor change in configuration, the novel reactor shows improvements in performance and cavitation ignition conditions.

1 INTRODUCTION

Clean water technology is a beacon of hope in the global pursuit of the Sustainable Development Goals of the United Nations, particularly in the context of water treatment.

In the current world, where water scarcity and contamination pose serious threats, innovative water treatment technologies are emerging as critical tools to mitigate these challenges.

Cavitation can be defined as the breakdown of a liquid medium under very low pressures. This makes cavitation relevant to the field of continuum mechanics and applies to cases in which the liquid is static or in motion. Bubble formation and growth are due to a sharp decrease in local pressure below the saturation pressure of the state. According to classical thermodynamics, saturation pressure refers to the pressure of a vapour in equilibrium with its liquid phase at a particular temperature, and both phases exist simultaneously. Once the bubbles reach a higher-pressure region, a violent collapse occurs, which is induced by the pressure difference between the internal and external frames. In fact, the internal pressure hardly varies and remains close to the saturation pressure. Rapid implosion generates intense

https://doi.org/10.52202/077185-0142

shock waves in the surrounding fluid. These shock waves are characterised by high-pressure gradients and can result in the release of energy in the form of acoustic waves and microjets. This effect is well known in turbomachinery for its erosive effects, damaging surfaces near low-pressure regions, and rapidly degrading the performance of components over time.

Cavitation is an intrinsically very complex phenomenon that must be studied, involving the intricate interplay of various physical and thermodynamic factors such as pressure fluctuations, multiphase flow, bubble dynamics, boundary layer effects, partial compressibility, and impact of structures. For this reason, it is useful to consider separately the different steps in the development of cavitation. Cavitation inceptions and cavitation development are considered equally distinguished. The first one identifies the limiting regime between the non-cavitating and cavitating flow, while the second is associated with the permanency of the cavity in the low pressure region. This distinction is crucial in accepting or rejecting cavitation in industrial systems. Deeper considerations about the effect of the pressure field on cavitation phases will be developed in the section design guidelines.

Essential for cavitating flow engineering is understanding the conditions that favour cavity development. Changes in wall geometry may lead to a sharp increase in local velocity, and resulting pressure drops within a globally steady flow. This is the case of cross-section restrictions (as in Venturi nozzles) or curvatures imposed on the flow streamlines locally (pipe flow, propellers, pumps, etc.). Generally, the unsteady nature of some flows can result in a strong acceleration of the fluid with consequent instantaneous production of low-pressure regions, leading at some points to cavitation.

Large turbulent flows and their shear flows could also give rise to pressure fluctuations; this is the case, for example, of jets, wakes, etc. In addition, the local roughness that characterises the pipe walls could produce local wakes but could also be active areas for the nucleation of the cavities.

The damaging effect of cavitation is often strongly emphasised. In many hydraulic systems, free cavitation represents the most severe and extremely challenging condition that designers have to deal with. However, we also experienced some industrial processes in which cavitation is exploited as an efficient way to concentrate energy on small surfaces, producing high-pressure peaks. Some processes that involve this positive effect of cavitation include dispersion, mixing, and emulsion of particles in a liquid medium. In addition, electrolytic deposition is preferred by the action of cavitation, which breaks down the ion layer that covers the electrodes, accelerating the deposition process. In the field of medical engineering, cavitation allows therapeutic massage and the destruction of bacteria (Gogate & Kabadi, 2009) (Dular, Khlifa, Fuzier, Maiga, & Coutier-Delgosha, 2012) (Biasiolo, Ballarin, Tassinato, Stoppato, & Cavinato, 2022) (Andrej Šarc, 2018). In aeronautic engine applications, the development of supercavities is exploited for the limitation of flow rates in confined flows. This feature is particularly relevant using some device configurations born in the flow measurement field (Bermejo, Escaler, & Ruìz-Mansilla, 2021).

Carpenter et al. (Carpenter, et al., 2016) sum up the theory of cavitation, focussing on the concept of "hot spots" generated by collapsing cavities, defined as strongly reactive points characterised by local temperatures of about 2300-4600k and pressures of 100-5000 bar (Song, Hou, Zhang, & Liu, 2022).

As a result of the formation of hydroxyl OH, degradation reactions are strongly favoured at these points. The available approaches to generate multiphase phenomena and the corresponding uses of the technology in different contexts are discussed later. The large space is given to the overview of many optimisation strategies developed through the theoretical analysis of experimental studies, which is helpful for the design and scale-up on the industrial level.

The increased reactivity associated with cavitation activity is the key reason for the high flexibility and potential demonstrated by this technology. An example of an application at the industrial level is the one described by Abbs-Shiroodi et al. (Abbas-Shiroodi, Sadeghi, & Baradaran, 2021) where the use of cavitating devices for Congo red decolorization is described, referring both to experimental and CFD investigations. Congo red is a widely used dye in the textile and plastic industries, whose release has a severe impact on aquatic ecosystems and human beings. In the reference paper, a comparison between geometrically different configurations is shown, highlighting a superiority in performances for the Venturi configuration with respect to single- and multi-hole cavitating devices. A maximum decolorization rate of 38% is reached, with the possibility of an improvement acting properly on the inlet pressure.

https://doi.org/10.52202/077185-0142

Another example is given by Bimestre et al. (Bimestre, Jùnior, Botura, Canettieri, & Tuna, 2020) describing a possible improvement in biomass degradation by means of a cavitation-based pretreatment. Hazardous environmental residue generation and high-energy input are the bottleneck of lignocellulosic biomass pretreatment processes. For this reason, there is an urgent need for solutions in green technologies in this field. A cavitation setup, incorporating a cavitating Venturi tube, was constructed on the basis of the results derived from computational modelling. The removal of lignin and the structural changes of bagasse can be attributed to the synergic effects of a combined pretreatment (hydrodynamic cavitation + alkaline solution).

One of the fields that shows the greatest potential and is one of our interests is water treatment. In particular, promising results could be achieved in the degradation of pollutants belonging to the polyfluoroalkyl (PFAS) family. PFAS are a hot topic nowadays; their widespread use in many industrial fields has led to consistent detection in the environment and in the human body. Some cavitation technologies have already shown good performance in PFAS depletion, reducing their concentration by approximately 70-90% (Kewalramani, Wang, Marsh, Meegoda, & Freire, 2022).

The ever-increasing growth of population and industrial activity inevitably stresses the need for clean water. Moreover, water treatment processes are known to be very energy expensive; for this reason, the development of some technologies able to purify water from cancerogenic substances using a minimal energy input is crucial today. To this end, the present paper seeks to provide a clear overview of how a relatively new technology could give a strong boost in a sector that will face many testing challenges in the future. Moreover, the contribution to the available knowledge involves the introduction of a device capable of exploiting cavitation for water purification, presenting a geometrically simple configuration but characterised by high energy efficiency and versatility of operation, together with the crucial points for a possible optimisation procedure.

2 CAVITATION DYNAMICS

As partially introduced in the previous section, cavitation phenomena are characterised by a high degree of complexity. From this we need to consider separately the different phases of bubble generation, growth, and collapse. A deep understanding of how bubble dynamics is influenced by the main flow parameters in the different phases could lead to a complete understanding of the overall cavitation phenomena.

In industrial applications involving the use of water as an operating fluid, we can currently assume the unperfect continuity of this homogeneous medium. These existing weak points are formed by persistent small gas or vapour particles. These points operate as starting points for cavitation and are known as cavitation nuclei. The existence of these points has been experimentally demonstrated, also verifying their size to be between a few micrometres and some hundreds of micrometres. Moreover, because of their surface tension, they maintain a spherical shape because of their surface tension (Franc & Michel, 2006) . In thermophilics, the assumptions of heterogeneities inside a homogeneous medium are very common in phase transfer, boiling, condensation, and condensations are clear examples. The surface of nuclei is usually made of gas trapped in small cavities, not filled by water, and for this reason, they are usually present on the surfaces of walls, but they can also be found in the bulk of liquids. It is easy to see that the wetting capacity of the liquid is of great importance. Consider also that the region downstream of developed cavities is an abundant source of nuclei, ultimately powering further cavitation phenomena (Franc & Michel, 2006). Generated nuclei can evolve remaining attached to the wall or being free to move in the fluid. Two main effects influence the nuclei evolution, gravity, promoting rise in absence of wall bounding, or exchange via diffusion with the dissolved gasses present in the surrounding liquid. Consider diffusion to be a very slow process, with typical timesteps of the order of seconds, much longer compared to the time necessary for bubbles to collapse, which takes milliseconds (Franc & Michel, 2006).

The void fraction resulting from the presence of free nuclei is extremely small, with a typical concentration of hundreds of nuclei per cubic centimetre (Franc & Michel, 2006). No appreciable changes are really involved in terms of the density and velocity of sound in the liquid.

https://doi.org/10.52202/077185-0142

Once a bubble is generated, we can consider it as a spherical microbubble containing vapour and gas. Equilibrium can be assumed at the interface with respect to the external fluid. Under these conditions, we can consider the following equation to be satisfied:

$$p = p_g + p_v - \frac{2S}{R} \tag{1}$$

where p_g is the partial pressure of the gas inside the bubble, S *is* the surface tension, R *is* the radius, and p is the pressure of the fluid.
Considering the evolution of an isolated nucleus, pressure variation represents the main driving force for bubble dynamics. The nuclei are characterised by a critical pressure value p_c below which the bubble interface becomes unstable. If the local pressure remains higher than p_c, the dimensions of the nuclei could slightly oscillate around the initial values, without notable changes. Instead, when the local pressure falls below the critical value, the nuclei become unstable and mush larger than the initial size. The evolution trend refers to the particular case but can be applied to many other flow configurations, paying attention to peculiar pressure variations, the time spent in the low pressure region, and the collapse time.
The simplest and most widely used model to investigate bubble dynamics is the Rayleigh-Plesset equation. It provides an easy non-linear ordinary differential equation, which governs the dynamics of spherical bubble in an infinitely incompressible fluid. Moreover, the theories involved can be easily scaled to different sizes or geometries. The Rayleigh-Plesset equation is formulated as follows.

$$\rho\left[R\,\frac{\partial^2 R}{\partial t^2} + \left(\frac{3}{2}\frac{\partial R}{\partial t}\right)^2\right] = [p_v - p_\infty(t)] + p_{g0}\left(\frac{R_0}{R}\right) - \frac{2S}{R} - 4\frac{\mu}{R}\frac{\partial R}{\partial t} \tag{2}$$

The left-hand side of the equation describes the change in the radius of the bubble using differential terms. On the right-hand side, the four different terms represent different driving forces that affect the dynamics of the radius. The first term is the most influential and represents the difference in pressure with respect to the vapour pressure. The second term quantifies the effect of noncondensable gases, which are often assumed to have constant mass during bubble evolution. The third term is the contribution of the surface tension coefficient, which is particularly relevant for smaller radii. The last term relates to the viscosity (μ) of the liquid within the bubble, which introduces a dissipative effect on the radial oscillation. Franc (Franc & Michel, 2006) explains that despite the simplicity of the equations and the complexity of the various regimes that can be recognised as an effect of interactions and turbulence, many basic results can be easily derived.
Along its path, the bubble becomes macroscopic as an effect of the permanence in the low-pressure region and finally collapses, reaching the zone where the pressure is recovered downstream.
In the bubble collapse phase, gas inside bubbles is assumed to behave as isothermal or adiabatic. Bubbles contain gas, mainly air and vapour. These are compressed when liquid rushes into the cavity; condensation may take place at the same time, and the collapse stops finally at a radius of the bubble so small that the pressure of thousands of atmospheres could be reached. Van Wijngaarden (Wijngaarden, 2016) exposes that, to give an idea, suppose that a bubble starts to collapse under a pressure difference of one bar far away and a pressure of 0.01 bar internal gas pressure at an initial radius of 1 mm. With a polytropic constant of 1.4, a minimum radius is reached of 1 μ and the final pressure is approximately $3 \cdot 10^7\ N/m^2$. The time required to reach the minimum radius is of order of 10^{-4} s.
Moreover, in practice, collapsing bubbles do not remain spherical because of the curvature of the interface, which causes the collapse instability. The interface would be stable if it were completely flat, with the heavy liquid accelerating into the lighter one. A rebound would follow in the case of unconfined surroundings, propagating strong shock waves in the liquid.
In conclusion, it is worth mentioning the two main mechanisms that lead to periodic shedding of bulk vapour. Because of differences in the adverse pressure gradient generated during the vapour flow, we could face re-entrant jet shading or bubbly shock wave shading. The topology of the re-entrant flow is such that a liquid film travelling upstream exists between the solid boundary and the vapour cavity, causing detachment of the latter. An example of re-entrant dynamics recreated with the model

 https://doi.org/10.52202/077185-0142

developed in this paper is reported in Figure 1. Bubbly shock regime exists for high values of the void fraction. If the void fraction front reaches the wedge apex, the vapour cloud is thrown away, and a shock wave is generated by the collapse of a large-scale cavity structure.

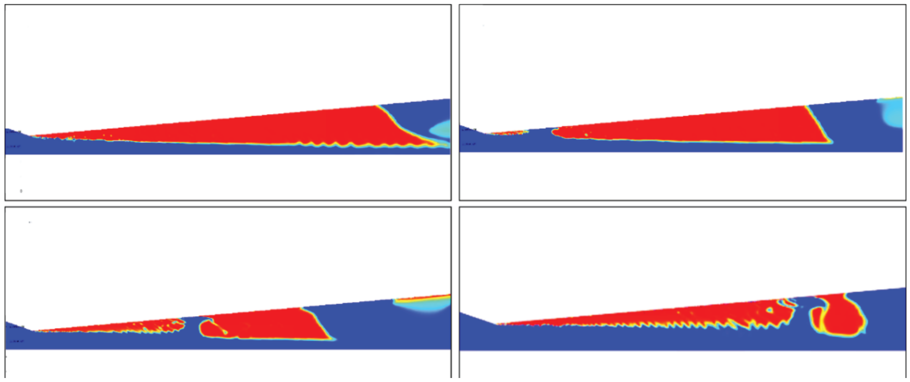

Figure 1: Vapour dynamics in the convergent-divergent section obtained with the implemented model.

3 DEVICES AND DESIGN

3.1 Choice of Technology

Originally, hydrodynamic cavitation was considered a possible alternative to ultrasonic cavitation (UC). Its exploitation has gained attention because of the improved energy efficiency and, above all, the capacity of this technique to work on larger-scale applications. The absence of a standardised methodology has transformed HC into a promising technology with inconsistent results.

Compared to ultrasonic cavitation, hydrodynamic cavitation is intrinsically more complex to induce and control.

Ultrasonic waves are produced through the resonant vibration of specific materials at a designated frequency, and consequently, intensity and pressure. On the contrary, the pressure pulse generated by HC is both quantitatively and qualitatively different. In HC, pressure pulses are the result of the generated liquid flow field, which is a function of the design of the cavitation chamber and the flow rate.

A commonly agreed assumption is that cavitation intensity and bubbles creation are directly related: Higher intensity implies a larger number of bubbles created and implosion events. However, according to some authors, excessive intensities lead to lower chemical activity. When the bubble cloud density becomes too large, coalescence and bubble-bubble interaction have a negative effect, decreasing overall efficiency of the process.

The pivotal difference between HC and UC is the time-scale reference for the two processes. Ultrasonic inducers can promote pressure oscillations with a much higher frequency, resulting in a greater amount of collapse per unit of time, strongly promoting the diffusion of OH radicals in the liquid phase.

Moreover, under these conditions, with a pressure oscillation period ranging between 1 and 50 ms, smaller bubbles form, which requires a higher intensity to grow. In addition to that, larger bubbles exhibit greater energy released, leading to a more powerful collapse. Therefore, operating at high frequency produces fewer energetic bubbles, but more collapsing cycles occur per unit of time.

By analogy, hydrodynamic cavitation can be seen as a lower frequency scenario (3 times longer time periods).

A lower cavitation threshold reduces the number of events per cycle, resulting in the generation of larger bubbles and consequently higher collapse temperatures. Furthermore, the diffusion of OH decreases, as does the number of cycles per unit time. These opposing effects combine to produce the highest chemical activity at intermediate frequencies. In summary, every cavitation process is characterised by growth and collapse phases, and the main factor that affects the collapse is pressure recovery, defined by both the pressure recovered and the time scale in which the recovery process takes place.

Taking now into account that the devices could be adopted to induce hydrodynamic cavitation, a wide range of possibilities is available in the literature: Venturi-type devices, single- and multiple-hole

https://doi.org/10.52202/077185-0142

orifices, vortex-based cavitation devices, aerofoils, etc. Sure, Venturi tubes and orifices are the simplest and most widely spread ones. Orifice-based geometries have the unique advantage of giving the possibility of using multiple element configurations. Depending on the number of orifices, the cavitation intensity could be modulated.

The configuration of our choice is the one of the Venturi tubes. Venturi-shaped nozzles are simple devices used in the field of flow measurement. At low-pressure operating points, cavitation exhibits increased stability due to its divergent wall configuration. Specifically, the cavitation section covers a much larger area than in the case of an orifice and is concentrated in the throttling region, with expansion occurring in the diverging section and a larger number of cavities. Moreover, the smooth section change allows us to achieve a lower cavitation number, for the same pressure drops.

3.2 Design Guidelines

The design of a Venturi tube is characterised by a large number of degrees of freedom with respect to the orifice case, as its geometry is defined by more than one parameter. Understanding the effect of individual measures is crucial for the design. From this point of view, computational fluid dynamics (CFD) techniques are considered master tools in cavitation analysis, allowing the effects of geometry changes in flow parameters. The modelling of cavitation phenomena interests a consistent part of the literature production in this field, developing one- and multidimensional models, under single and multiphase conditions (Bashir, Soni, Mahulkar, & Prandit, 2011) (Dastane, et al., 2019). The results obtained focus on the limits of single-phase modulizations with respect to two-phase ones in the flow analysis, highlighting the main parameters for configuration evaluations and exposing some possible optimisation routines suitable for this kind of geometry. Tang, Juàrez and Li. (Tang, Juàrez, & Li, 2019) expose a clear overview of the influence of Venturi geometry on cavitation capacity through experimental and numerical analysis. The author highlights that the convergent angle does not have a huge impact in the cavitation area, while the divergent angle does.

In summary, the outlet angle and the diameter ratios are found to be the two key parameters in controlling throat pressure and power consumptions.

Moreover, literature gives us some dimensionless numbers expressing the resistance given by configuration and the intensity of cavitation (exposed in section *Results*) From the exploration of their trends and values we can identify working regimes and inception conditions.

Despite the already existing work, the prediction of cavitation dynamics using numerical models is still a critical issue. The basin of information made available from the literature is still not sufficient to define an organic optimisation procedure for the design of these kinds of device. The aim of our work is to solve this knowledge gap. From a deep understanding of the cavitation phenomena, we can develop a numerical model that defines the performance of a baseline reference configuration. Once good agreement of the results with the experimental data is demonstrated, the model is used to study a novel optimised configuration aimed at simplifying the manufacturing process and implementation of a possible multireactor device.

In conclusion, it is worth specifying that even if the most accurate results are obtained by adopting the most advanced CFD strategies, such as Large-Eddy Simulations (LES) and Direct Numerical Simulations (DNS), the high computational effort required by these kinds of simulations makes them a high-potential but low-efficient instrument at industrial level. Therefore, digital prototyping of such devices is still demanded by Reynolds-Averaged Navier-Stokes (RANS) based models, albeit with all the limitations that such strategy embeds. We have decided to adhere to this standard and propose a tool that is both flexible and easy to operate.

4 COMPUTATIONAL SETUP

The development of a properly calibrated numerical model requires first the definition of a baseline geometry for which reference experimental data are made available. To this end, the University of Padova research group (Turbomachinery and Energy Systems - TES Group), after an in-depth review of the literature, has selected the baseline geometry configuration of the Venturi tube (De Vanna, Benato, Scramoncin, & Stoppato, 2022) proposed by Shi et al. (Shi, Li, Nikrityuk, & Liu, 2019).

https://doi.org/10.52202/077185-0142

A schematic representation of the baseline case is reported in Figure *2* while the value of the dimensions is reported in Table *1*.

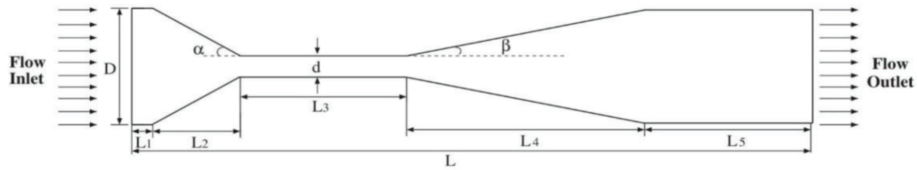

Figure 2: Schematic view of the Venturi tube geometry. Dimensions are listed in Table 1.

Table 1: Geometry characteristics of the baseline shape of the Venturi tube as given by (Shi, Li, Nikrityuk, & Liu, 2019)

D (mm)	**d** (mm)	**L_1** (mm)	**L_2** (mm)	**L_3** (mm)	**L_4** (mm)	**L_5** (mm)	**α** (°)	**β** (°)
12.7	3.18	6.00	14.00	20.0	54.0	6.00	19.0	5.00

Based on the knowledge acquired by the TES research group and the axial symmetry of the geometry, we decided to limit the task to a 2D domain. Ansys-Workbench 2022 R1 (Ansys, 2022) is used to build both geometry and grids, while Ansys-Fluent is used to solve the flow field. The structured mesh adopted for the model was built based on the experience of the research team in the field of CFD, performing a detailed sensitivity analysis (see (De Vanna, Benato, Scramoncin, & Stoppato, 2022). Different mesh sizes were tested with the aim of finding the best compromise between the accuracy of the results and the efficiency of the calculation. Researchers have paid particular attention to ensuring proper values of element sizes, and a proper refinement of the layers near the wall ensures an accurate value of the wall Y plus. A detailed description of the mesh is presented in Figure *3*.
The solution is researched in an incompressible RANS system of equations and transient framework. The analysis performed by the TES research group (De Vanna, Benato, Scramoncin, & Stoppato, 2022) also highlighted that with increasing complexity of the turbulence model, no appreciable differences are observed. For this reason, the k-omega shear stress transport (SST) model is applied.

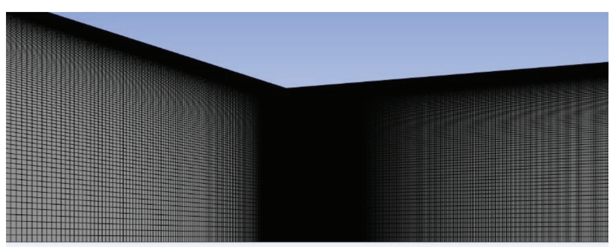

Figure 3: Detail of the refinement of the mesh adopted for the optimised convergent-divergent Venturi case in the throat region

The other sub-models chosen for implementation in our model are reported in Table 2.

Table 2: Resume of the models used in the analysed model from Ansys.

Name	**Model/scheme name**
Multiphase flow	Volume of fluid
Volume fraction parameters	Implicit Scheme
Viscous model	k-ω SST
Cavitation model	Schnerr-Sauer
Pressure-Velocity Coupling	Coupled scheme
Spatial Diskretization Gradient	Least squares cell-based
Spatial discretization-pressure	PRESTO!
Spatial discretization-momentum	Second-order upwind

https://doi.org/10.52202/077185-0142

Spatial discretization-volume fraction	QUICK
Spatial discretization-turbulence	k-ω 2nd-Order Upwind

5 RESULTS

5.1 Validation of the Model

In the field of fluid dynamics, we refer to some characteristic parameters, essential to quantify and understand fluid behaviour, enabling accurate predictions of flow patterns and optimisation of fluid systems. *The Cavitation Number* σ has been recognised as the basis for the evaluation of potential cavitation applications. It is a dimensionless number that expresses the relationship between the difference of a local absolute pressure from the vapour pressure and the kinetic energy per unit of volume, and it is used to characterise the potential cavitation.
It can be expressed as:

$$\sigma = \frac{p - p_v}{\frac{1}{2}\rho V^2} \tag{3}$$

where p is the centerline absolute pressure, p_v is the saturated vapour pressure of the fluid at operation temperature, and V is the speed of the fluid. The coefficient σ decreases with increased probability of cavitation. Moreover, it is crucial to note that, assuming the same outlet pressure, the number of cavitations depends only on the throat speed, which in turn is a function of the flow area of the cross section of the throat. In other words, the cavitation number cannot be used alone as a measure of the performance of the phenomenon. In addition to that, another dimensionless parameter is used, with similar characteristics and meaning*: Resistance number* or *Loss coefficient L_c*.

$$L_c = \frac{p_{in} - p_d}{\frac{1}{2}\rho V^2} \tag{4}$$

where the same symbology is maintained as before and p_{in} is the pressure at the input and p_d the pressure at the discharge section. In this case, we represent the pressure drop associated with the cavitating component with respect to the kinetic energy involved.
None of these two parameters alone can give a complete description of the cavitation phenomenon. Therefore, the focus is moved to possible relationships between them. This relationship is known in the literature. We have reported it in

Figure **4**. Two different zones can be well distinguished: the cavitation area and the non-cavitation area. When the working position moves from one to another, indicating the beginning of cavitation, a discontinuity is observed. The profile knee distinguishes the cavitation region (on the left) from the non-cavitation zone (on the right).

In the single-phase fluid region, the loss coefficient L_c assumes a constant value as σ changes. Once the incipient cavitation conditions have been reached, there is an increase in the loss coefficient Lc, due to

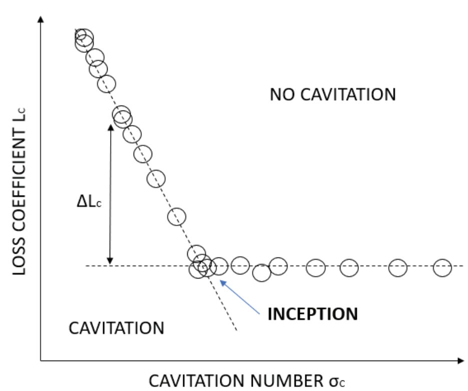

Figure 4: Trenc itation number.

https://doi.org/10.52202/077185-0142

the change in the liquid-vapour state, which increases linearly as the cavitation number decreases. The physical explanation of this trend can be given as follows: as the discontinuity in the curves individuates the incipient cavitation conditions, we can consider that the higher the value of the cavitation number for which cavitation starts, the lower the resistance number, and consequently, the easier it is to cavitate. The resistance number can be seen as a measure of the resistance imposed by our configuration to cavitation. Having a configuration with low resistance number causes cavitation to begin with a higher cavitation number, and so with a higher discharge pressure.

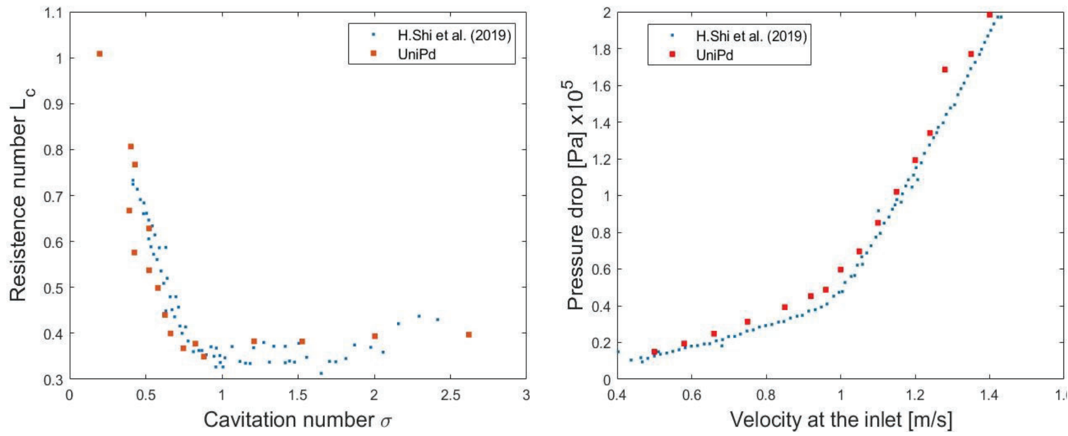

Figure 5: Characteristic curves evaluated by experimental data and developed model for the baseline configurations.

The validation of the model developed is based on the experimental data provided by Shi et al. (Shi, Li, Nikrityuk, & Liu, 2019). The authors report values of the Loss Coefficient Lc as a function of the Cavitation Number σ, as reported in

Figure **5**. In addition, pressure drop values are also defined as a function of inlet velocity. These two sets of data are taken as a reference to define the accuracy of our model.

Different operating conditions are discussed, modifying the boundary values, and confirming the consistency of the results with the expected cavitation regimes. An example of the velocity, pressure, and volume fraction regimes obtained is reported in

Figure **6**.

In Figure 5 we can see the reference data reported together with the results of the model developed by the research group. Focussing on the first of the two charts, the results obtained with the simulations follow the expected trends described above. However, we still had to notice that we were unable to obtain a perfect superposition of our results with the experimental data. The numerical curves remain on the left side compared to the reference data, representing the tendency of the model to underestimate the resistance number for the same cavitation number.

In addition, we must take into consideration that our model tends to slightly anticipate the passage between cavitation and non-cavitation regimes. The experimental data show a discontinuity in the data distribution for a cavitation number of about 0.8, while in our model the transition occurs at a cavitation number of about 0.75.

Taking into account the results reported in the second graph in

Figure **5** the precision of the pressure drop values evaluated with the new model can be verified. When comparing the two sets of data, we can clearly see that the trend obtained experimentally is also maintained by our simulations. A clear separation, identified by a threshold inlet velocity of about 1 m/s, separates the operative conditions analysed. In both regions, pressure drops increase with an increase in the inlet velocity. However, above the threshold value, the increase is much more accentuated.

For a lower inlet velocity and therefore higher inlet pressures, simulations have shown no vapour generation. Under these conditions, the velocity and pressure profiles do not show high irregularities

https://doi.org/10.52202/077185-0142

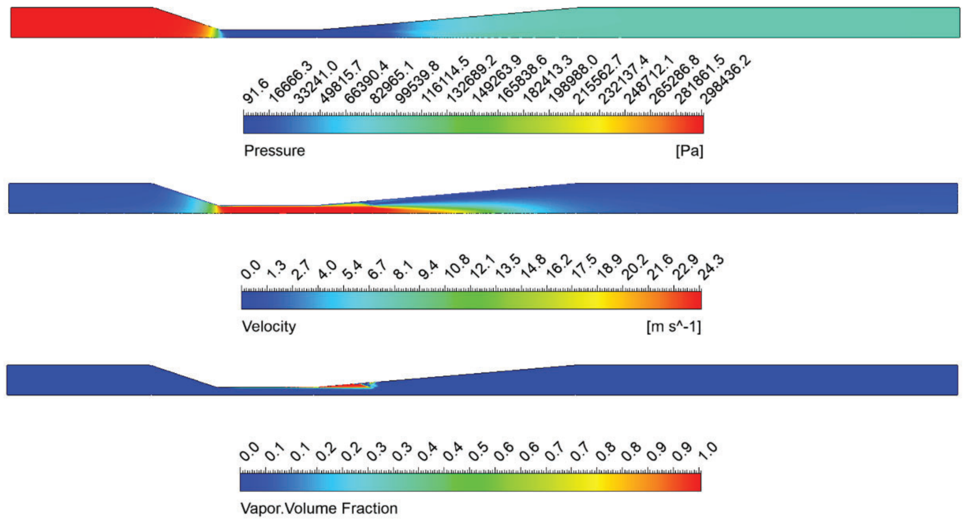

Figure 6: Example of pressure, velocity and volume fraction trends obtained with the model.

with a low turbulent effect. Together with that, since the Venturi profile is not very sharp, the liquid flow will be well directed, avoiding massive dissipative effects such as the detachment of the boundary layer.

For a higher inlet velocity and, therefore, lower inlet pressure, simulations have shown cavitation generation. Under these conditions, the velocity and pressure profiles tend to be irregular not only in the Venturi section but also in time, because of the periodicity of the cavitating phenomena. Moreover, the reentrant jet mechanism causes velocity and pressure variations that promote turbulence, increasing pressure drops. For this reason, the higher slope of the pressure drop curve in the cavitating region appears to be consistent with the flow field generated inside the Venturi pipe.

Lastly, even if the trends obtained show consistency with the experimental results, the model slightly overestimates pressure drops, but still does not exceed about 3-4% under critical conditions.

In conclusion, the congruence between numerical predictions and real-world observations underscores the robustness of our methodology and strengthens confidence in the validity of our model.

5.2 Alternative Configuration

Once the validation of the developed model is completed, another step in the investigation involves its use to study the performance of a new optimised configuration. Taking into account the functional destination of the research technology, the new configuration aims to overcome possible problems resulting from the peculiar shape and dimensions of the device. These aspects become very limiting in the manufacturing process and require highly specialised equipment. On the basis of that, a converging-diverging configuration is proposed. A representation of the new geometry is shown in Figure *7*.

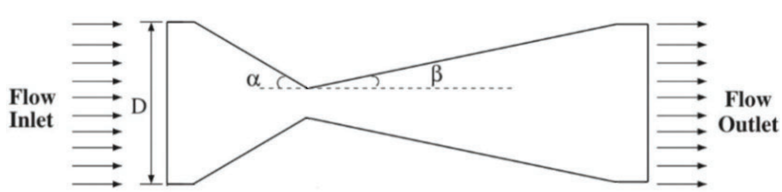

Figure 7: Schematic view of the new divergent-convergent configuration.

The nozzle is characterised by the correspondence dimension with respect to the baseline configuration, reported in Table 1. with the only difference of removing the throat region. In the literature, different

https://doi.org/10.52202/077185-0142

examples of no-throat-shaped cavitating devices can be found, chosen mainly for their simplicity and possibility of implementing multielement configurations.

However, our work, having the peculiarity of comparing two twin configurations, gives information not only on the single performances of the devices but also on the effect of the throat length variation on cavitation rise.
As in the baseline configuration, different working conditions are reproduced using the validated model to recreate the main characteristic curve for the novel configuration. The results are described in 8.

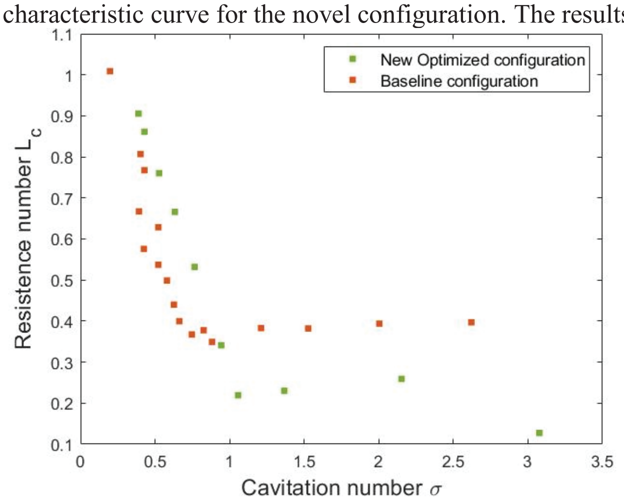

Figure 8: Resistance rate and cavitation rate for baseline and optimised geometry.

As can be clearly observed, the characteristic curve for the novel configuration shows a trend of resistance number, which is well close to the expected behaviour from the literature.
Figure *4*). The direction identified by the cavitating points for low cavitation number is comparable with the one obtained under cavitation conditions by the baseline configuration, being essentially parallel. The same effect can be also observed for the non-cavitating region.
Nevertheless, the difference between the two characteristic curves and consequently the two configurations lies in the relative position: the novel configuration presents a characteristic shifted downward. Physically, this difference is related to pressure drops generated under comparable conditions. For the same value of the Cavitation number σ, which is identified by the velocity of the fluid in the configuration, the new configuration develops a lower Resistance number L_C. Returning to the definition of this parameter, the reduction in this parameter is associated with a lower pressure drop generated by the configuration under cavitating conditions, assuming the same velocity in the throat. However, a possible contribution of velocity variation on the parameter must also be taken into consideration. In particular, defining the reference velocity at the throat in the absence of a constant cross-section region is particularly difficult and not very precise. Moreover, the presence of vapour alters the liquid flow field in terms of the velocity of the low-pressure area. These effects strongly influence the full throat configuration in terms of obstruction of the flow passage area and local increase in velocity. Instead, in the convergent-divergent case, these effects remarkably destabilise the flow.
Furthermore, by focussing on the cavitation inception conditions, it is reached for Cavitation number very close to 1, slightly higher than for the baseline configuration, showing the incipiency at about σ= 0.8. This result demonstrates a notable improvement in the achievement of cavitation. Indeed, in this way a more precise control and manipulation of the cavitation process is allowed. This finer control over cavitation dynamics can lead to increased efficiency, reliability, and effectiveness in various applications.

6 CONCLUSIONS

The present work aims to give prominence to a promising technology that is already showing good results in the field of water treatment, but its potential energetic improvements could apply to a wide

https://doi.org/10.52202/077185-0142

range of industrial processes. To do that, an in-depth discussion about the nature of the phenomenon and its fluid dynamics is performed, also bringing some examples of emblematic applications from the literature. The investigation in the cavitation field proceeds with the proposal of a numerical model suitable for the evaluation of the performances of a Venturi-based geometry. The model is calibrated by considering a baseline configuration for which experimental data is available. Once the model is verified, we have been able to analyse a new configuration, enhancing improvements in terms of flexibility and operations.

REFERENCES

Abbas-Shiroodi, Z., Sadeghi, M.-T., & Baradaran, S. (2021). Design and optimization of a cavitating device for Congo red decolorization: Experimental investigation and CFD simulation. *Ultrasonic Sonochemistry*.

Andrej Šarc, J. K. (2018). Removal of bacteria Legionella pneumophila, Escherichia coli, and Bacillus subtilis by (super)cavitation. *Ultrasonic Sonochemistry*, 228-236.

Ansys. (2022). *FLUENT 12.0 Theory Guide.* Tratto da https://www.afs.enea.it/project/neptunius/fluent/html/ug/node1.htm

Bashir, T. A., Soni, A. G., Mahulkar, A. V., & Prandit, A. B. (2011). The CFD driven optimisation of a modified venturi for cavitational activity. *The Canadian Journal of Chemical Engineering, 89*(6), 1366-1375.

Bermejo, D., Escaler, X., & Ruìz-Mansilla, R. (2021). Experimental investigation of cavitating Venturi and its application to flow metering. *Flow Measurement and Instrumentation*.

Biasiolo, M., Ballarin, M., Tassinato, G., Stoppato, A., & Cavinato, C. (2022). Semi-continuous Chlorella Vulgaris Cultivation Using Anaerobic Digestate Liquid Fraction Pre-treated by Ultrasonic Cavitation to Improve Carbon Dioxide Solubilization. *CEt Chemical Engineering Transactions* , 151-156.

Bimestre, T. A., Jùnior, J. A., Botura, C. A., Canettieri, E., & Tuna, C. E. (2020). Theoretical modeling and experimental validation of hydrodynamic cavitation reactor with a Venturi tube for sugarcane bagasse pretreatment. *Bioresource Technology, 311*.

Carpenter, J., Badve, M., Rajoriya, S., George, S., Saharan, V. K., & Pandit, A. B. (2016). Hydrodynamic cavitation: an emerging technology for the intensification of various chemical and physical processes in a chemical process industry. *Reviews in Chemical Engineering*, 433-468.

Dastane, G., Thakkar, H., Shah, R., Perala, S., SRault, J., & Pandit, A. B. (2019). Single and multiphase CFD simulations for designing cavitating venturi. *Chemical Engineering Research and Design*(149), 1-12.

De Vanna, F., Benato, A., Scramoncin, A., & Stoppato, A. (2022). CFD modelling of a Venturi tube for wastewater treatment applications. *Proceedings of ECOS 2022 - 35th International Conference on Efficiency, Cost, Optimization, Simulation and Environmental Impact of Energy Systems*.

Dular, M., Khlifa, I., Fuzier, S., Maiga, M. A., & Coutier-Delgosha, O. (2012). Scale effect on unsteady cloud cavitation. *Experiments in fluids*, 1233-1250.

Franc, J.-P., & Michel, J.-M. (2006). *Fundamentals of Cavitation* (Vol. 76). Kluwer Academic Publishers.

Gogate, P. R., & Kabadi, A. M. (2009). A review of applications of cavitation in biochemical engineering/biotechnology. *Biochemical Engineering Journal, 44*(1), 60-72.

Kewalramani, J. A., Wang, B., Marsh, R. W., Meegoda, J. N., & Freire, L. R. (2022). Coupled high and low-frequency ultrasound remediation of PFAS-contaminated soils. *Ultrasonic Sonochemistry, 88*.

Shi, H., Li, M., Nikrityuk, P., & Liu, Q. (2019). Experimental and numerical study of cavitation flows in venturi tubes:. *Chemical Engineering Science*, 672-687.

Song, Y., Hou, R., Zhang, W., & Liu, J. (2022). Hydrodynamic cavitation as an efficient water treatment method for various sewage:- A review. *Water Science and Technology*(86), 302-320.

Tang, P., Juàrez, J. M., & Li, H. (2019). Investigation on the Effect of Structural Parameters on Cavitation Characteristics for the Venturi Tube Using the CFD Method. *Water*, 2194.

https://doi.org/10.52202/077185-0142

Wijngaarden, L. v. (2016). Mechanics of collapsing cavitation bubbles. *Ultrasonic Sonochemistry*, 524-527.

https://doi.org/10.52202/077185-0142